Experiments and Analysis for Composite Blades Under Large Deflections Part I: Static Behavior

Pierre Minguet* and John Dugundji†
Massachusetts Institute of Technology, Cambridge, Massachusetts 02139

The static behavior of structurally coupled composite blades is investigated analytically and experimentally in this paper. A model, based on the use of Euler angles, is developed that can account for the presence of arbitrarily large deflections without the need for any ordering scheme. A simple iterative finite-difference solution procedure is then presented. Some experiments using thin flat composite cantilevered beams are also performed, and the data obtained compare well with the results from the analysis.

Introduction

In recent years, composite materials have emerged as a primary material for helicopter rotor blades and are showing great promise for improved performance in a new generation of helicopters. However, as with the introduction of any new technology, a large amount of basic research is needed in order to obtain a better understanding of the new problems created by the use of composite materials. One such problem of interest here is the presence of structural couplings such as extension-twisting and bending-twisting that can be used to improve the dynamic and aeroelastic performance of helicopter rotors.[1-3] Another problem is to develop an analytical model to describe the static and dynamic behavior of long flexible blades. Initial work on the subject focused first on obtaining a set of equations capable of describing the linear coupled bending and twisting behavior of nonuniform blades.[4,5] However, it has been shown that nonlinearities can be important in calculating the dynamic response and aeroelastic stability of hingeless rotors.[6,7] Several approaches have been taken to study that aspect, with much work having been done to develop sets of equations including nonlinear terms of various orders. Most of these procedures rely on some ordering scheme, which can become quite involved algebraically, in trying to determine which terms are to be retained and some uncertainty always as to the accuracy of the procedure.[8-10] Recently, some work has also been done using the finite-element method for the nonlinear behavior of rotor blades.[11,12]

In this paper, a new model based on the use of Euler angles, without any limitation on the magnitude of displacements, is presented. A simple and fast finite-difference solution procedure is introduced and illustrated with a few examples. These analytical results are then compared with experimental data obtained for several cantilevered graphite/epoxy thin blades. More detailed analytical and experimental results from this study can be found in Ref. 13.

Analysis

The major part of the analysis is to develop a model for the large (nonlinear) static deflection behavior of beams with various kinds of structural couplings such as extension-twist and bending-twist. While presenting first all of the necessary equations, some of the basic assumptions of the classical theory of beams will be briefly recalled and those that need to be modified in order to analyze the large deflection behavior of beams will be indicated. The first assumption of the classical theory is that the beam is much longer in one direction and its cross section is undeformable and therefore will not change shape under load. This allows one to reduce the problem to a one-dimensional model in which all displacements are a function of only one coordinate, namely, the beam arc length s measured along some reference line. This assumption is usually true for most helicopter rotor blades and will therefore be retained here.

Therefore, the beam position in space can be completely described by the position of its reference line. As shown in Fig. 1, two coordinate systems are introduced. The first one (x, y, z) will hereafter be referred to as the global coordinate system that will remain fixed in space at all times; the second one (ξ, η, ζ) is the local axes system that will follow the beam cross section during its motion. For the time being, it will be assumed that the transverse shear strains in the cross section are not significant so that we can presume the cross section remains orthogonal to the reference line at all times. With this assumption, it follows that the ξ axis will be both normal to the cross section and tangent to the reference line. The other two axes η and ζ then belong to the plane of the cross section and can be chosen arbitrarily.

In order to describe the deformation of the beam in space, the reference line position is identified by its three displacements u, v, w measured along the global axes. The attitude of the cross section, and thus of the local axes system, is described with the use of the three Euler angles ψ, β, θ as shown in Fig. 1. In order to go from the global to local axes, rotations are done in the following order: ψ around the ζ axis, β around the new η axis, and θ around the new ξ axis. A transformation matrix from the global to local axes system is then defined as

$$\begin{bmatrix} i_\xi \\ i_\eta \\ i_\zeta \end{bmatrix} = [T] \begin{bmatrix} i_x \\ i_y \\ i_z \end{bmatrix} \tag{1}$$

where i_x, i_y, i_z are the global axes base vectors, i_ξ, i_η, i_ζ are the local axes base vectors, and $[T]$ is the transformation matrix.

The transformation matrix can be obtained by performing the three individual rotations in the order just indicated. All multiplications complete, the transformation matrix is

$$[T] = \begin{bmatrix} \cos\beta\cos\psi & \cos\beta\sin\psi & \sin\beta \\ -\cos\theta\sin\psi & +\cos\theta\cos\psi & \sin\theta\cos\beta \\ -\sin\theta\sin\beta\cos\psi & -\sin\theta\sin\beta\sin\psi & \\ +\sin\theta\sin\psi & -\sin\theta\cos\psi & \cos\theta\cos\beta \\ -\cos\theta\sin\beta\cos\psi & -\cos\theta\sin\beta\sin\psi & \end{bmatrix} \tag{2}$$

Received April 13, 1989; revision received Aug. 7, 1989.

*Research Assistant, Technology Laboratory for Advanced Composites, Department of Aeronautics and Astronautics.

†Professor, Department of Aeronautics and Astronautics. Member AIAA.

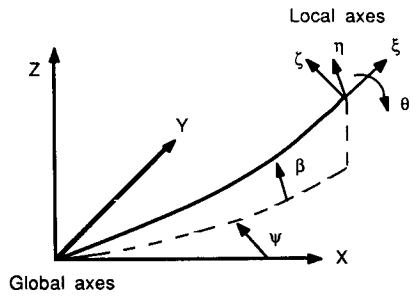

Fig. 1 Global and local axes.

Also, as for all rotation matrices, the inverse of the rotation matrix is equal to its transpose and is also the rotation from the local to global axes

$$[T]^{-1} = [T]^T \tag{3}$$

When moving the local coordinate system along the reference line from a point s to a point $s + ds$, the local axes (ξ, η, ζ) undergo a small rotation and the change in the transformation matrix is given by the following rotation:

$$\frac{d[T]}{ds} = [\omega]\,[T] \tag{4}$$

with

$$[\omega] = \begin{bmatrix} 0 & \omega_\zeta & -\omega_\eta \\ -\omega_\zeta & 0 & \omega_\xi \\ \omega_\eta & -\omega_\xi & 0 \end{bmatrix}$$

where ω_ξ is the twist rate, ω_η the bending curvature around η axis, and ω_ζ the bending curvature around ζ axis. After post-multiplying both sides of the equation by $[T]^{-1}$ and taking the derivatives of $[T]$, we obtain the following relations:

$$\omega_\xi = \frac{d\theta}{ds} + \sin\beta\,\frac{d\psi}{ds} \tag{5a}$$

$$\omega_\eta = -\cos\theta\,\frac{d\beta}{ds} + \sin\theta\cos\beta\,\frac{d\psi}{ds} \tag{5b}$$

$$\omega_\zeta = \sin\theta\,\frac{d\beta}{ds} + \cos\theta\cos\beta\,\frac{d\psi}{ds} \tag{5c}$$

The next step in beam theory is usually to write equilibrium equations for a differential element of the beam reference line. for the classical theory of beams, in order to keep the equations linear, equilibrium equations for a section of the beam are written in the beam undeformed position, so that stresses and displacements are not directly coupled in the equilibrium equations. The present model has to differ on this point since in the large deflection problem, it is necessary to take into account the beam deformed position in space while evaluating equilibrium equations.

On each cross section, it is further assumed that the internal stresses can be defined by their resultant force and moment vector that are defined in the cross section local coordinates

$$\boldsymbol{F} = F_1\boldsymbol{i}_\xi + F_2\boldsymbol{i}_\eta + F_3\boldsymbol{i}_\zeta \quad \text{or} \quad \boldsymbol{F} = (F_1, F_2, F_3)^T \tag{6a}$$

$$\boldsymbol{M} = M_1\boldsymbol{i}_\xi + M_2\boldsymbol{i}_\eta + M_3\boldsymbol{i}_\zeta \quad \text{or} \quad \boldsymbol{M} = (M_1, M_2, M_3)^T \tag{6b}$$

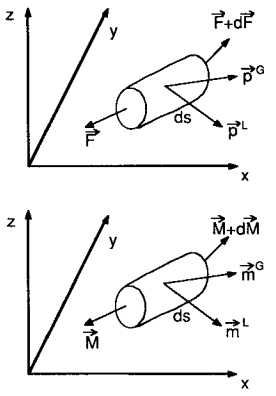

Fig. 2 Force and moment equilibrium.

Equilibrium equations can then be written by considering an infinitesimal element of beam of length ds with forces $\boldsymbol{F}$ and moment $\boldsymbol{M}$ acting on one side and $\boldsymbol{F} + d\boldsymbol{F}$ and $\boldsymbol{M} + d\boldsymbol{M}$ on the other side as shown in Fig. 2. Because of the large deflections and rotations, two types of distributed forces and moment are considered as applied on this element: The first type represents loads that are measured in the global coordinate system and the second type represents loads that are measured in the local coordinate system. For example, gravity loads should always be measured in global axes and aerodynamic loads should be used in local axes. Thus, writing first the translation equilibrium in global axes, we obtain following three equations

$$-[T]^T\boldsymbol{F} + ([T] + [dT])^T(\boldsymbol{F} + d\boldsymbol{F}) + [T]^T\boldsymbol{p}^L ds + \boldsymbol{p}^G ds = 0$$

where $\boldsymbol{p}^L$ is the load vector in local axis and $\boldsymbol{p}^G$ the load vector in global axis. If we premultiply by $[T]$ and use Eq. (4), the final equations are

$$\frac{d\boldsymbol{F}}{ds} + [\omega]^T\boldsymbol{F} + \boldsymbol{p}^L + [T]\boldsymbol{p}^G = 0 \tag{7}$$

Or, if we expand this matrix equation, three scalar first-order differential equations can be written

$$\frac{dF_1}{ds} - \omega_\zeta F_2 + \omega_\eta F_3 + p_1^L + T_{11}p_1^G + T_{12}p_2^G + T_{13}p_3^G = 0$$

$$\frac{dF_2}{ds} + \omega_\zeta F_1 - \omega_\xi F_3 + p_2^L + T_{21}p_1^G + T_{22}p_2^G + T_{23}p_3^G = 0$$

$$\frac{dF_3}{ds} - \omega_\eta F_1 + \omega_\xi F_2 + p_3^L + T_{31}p_1^G + T_{32}p_2^G + T_{33}p_3^G = 0$$

Similarly, the moment equilibrium can be written around the left side of the beam element

$$-[T]^T d\boldsymbol{M} + ([T] + [dT])^T(\boldsymbol{M} + d\boldsymbol{M}) + [T]^T[d\bar{r} \times (\boldsymbol{F} + d\boldsymbol{F})] + [T]^T\boldsymbol{m}^L ds + \boldsymbol{m}^G ds = 0$$

where

$\boldsymbol{m}^L$ = applied moment in local axis
$\boldsymbol{m}^G$ = applied moment in global axis
$d\bar{r} = (ds, 0, 0)^T$, $\quad t = d\bar{r}/ds$ unit tangent

If we premultiply by $[T]$, the final equations are

$$\frac{d\boldsymbol{M}}{ds} + [\omega]^T\boldsymbol{M} + (t \times \boldsymbol{F}) + \boldsymbol{m}^L + [T]\boldsymbol{m}^G = 0 \tag{8}$$

Expanding this relation in scalar form gives the following first-order differential equations:

$$\frac{dM_1}{ds} - \omega_\zeta M_2 + \omega_\eta M_3 + m_1^L + T_{11}m_1^G + T_{12}m_2^G + T_{13}m_3^G = 0$$

$$\frac{dM_2}{ds} + \omega_\zeta M_1 - \omega_\xi M_3 - F_3 + m_2^L + T_{21}m_1^G + T_{22}m_2^G + T_{23}m_3^G = 0$$

$$\frac{dM_3}{ds} - \omega_\eta M_1 + \omega_\xi M_2 + F_2 + m_3^L + T_{31}m_1^G + T_{32}m_2^G + T_{33}m_3^G = 0$$

Note that these equilibrium equations are nonlinear in two respects: First, the curvature tensor $[\omega]$ is a function of the internal force and moment vector so that the second term in the equilibrium equations is actually a quadratic-type term. Second, the loading may depend on the deformation, that is, on the three Euler angles that appear in the transformation matrix $[T]$. These nonlinear force and moment equilibrium equations in local coordinates are similar to those given by, among others, Rivello in Ref. 14.

As in any structural mechanics model, the next group of equations necessary to the solution of the problem is a series of compatability equations relating the generalized strains to the displacements, which, in this model, are the curvatures and Euler angles, respectively. When we go back to Eqs. (5) and invert them, the following relations are found:

$$\frac{d\theta}{ds} = \omega_\xi - \sin\theta \tan\beta\, \omega_\eta - \cos\theta \tan\beta\, \omega_\zeta \tag{9a}$$

$$\frac{d\beta}{ds} = -\cos\theta\, \omega_\eta + \sin\theta\, \omega_\zeta \tag{9b}$$

$$\frac{d\psi}{ds} = \frac{\sin\theta}{\cos\beta}\omega_\eta + \frac{\cos\theta}{\cos\beta}\omega_\zeta \tag{9c}$$

Note that these equations will become singular for $\beta = \pi/2$, which indicates that Euler angles cannot be used if a segment of the beam is parallel to the z axis. For practical purposes, this is not considered a serious limitation for the kind of beams that will be analyzed in this study. Note, however, that other similar representations are available that overcome this limitation of Euler angles, such as Euler parameters or Rodrigues parameters.[12]

Another set of compatability equations relates displacements and Euler angles using the transformation matrix

$$\begin{bmatrix} dx \\ dy \\ dz \end{bmatrix} = [T]^T \begin{bmatrix} (1+\epsilon)\, ds \\ 0 \\ 0 \end{bmatrix}$$

where ϵ is the axial strain along the reference line. Expanding this also gives three first-order differential equations

$$\frac{dx}{ds} = (1+\epsilon)\cos\beta\cos\psi \tag{10a}$$

$$\frac{dy}{ds} = (1+\epsilon)\cos\beta\sin\psi \tag{10b}$$

$$\frac{dz}{ds} = (1+\epsilon)\sin\beta \tag{10c}$$

where x, y, z represent the coordinates of the deformed reference line.

The last relations needed to complete the system of equations are a set of generalized stress-strain relations. In its most general form, they can include couplings between all six stresses, i.e., the three force resultants and the three moment resultants, and all six strains, i.e., the axial strain, the two transverse shear strains, the twist rate, and the two bending curvatures.

$$\begin{bmatrix} F_1 \\ F_2 \\ F_3 \\ M_1 \\ M_2 \\ M_3 \end{bmatrix} = \begin{bmatrix} E_{11} & E_{12} & E_{13} & E_{14} & E_{15} & E_{16} \\ & E_{22} & E_{23} & E_{24} & E_{25} & E_{26} \\ & & E_{33} & E_{34} & E_{35} & E_{36} \\ & & & E_{44} & E_{45} & E_{46} \\ & \text{SYM} & & & E_{55} & E_{56} \\ & & & & & E_{66} \end{bmatrix} \begin{bmatrix} \epsilon \\ \gamma_{\xi\eta} \\ \gamma_{\xi\zeta} \\ \omega_\xi \\ \omega_\eta \\ \omega_\zeta \end{bmatrix} \tag{11}$$

In this notation, E_{44} represents torsional stiffness, E_{55} and E_{66} bending stiffnesses, etc.

Solution Procedure

All of the necessary equations have now been obtained for the static large deflection model. Everything considered, there are 12 unknowns, i.e., three force components, three moments, three angles, and three displacements, after eliminating the curvatures and strains by the inverted stress-strain relations (11). Corresponding to these 12 unknowns, there are also 12 first-order nonlinear differential equations, namely, Eqs. (7-10).

To solve this system, these equations are first discretized by dividing the beam into a finite number of nodes (N) and using centered finite-difference formulas to represent derivatives. For instance, for the first group of force equilibrium equations written as

$$\frac{dF_k}{ds} + G_k = 0 \qquad k = 1, 2, 3$$

one obtains

$$\frac{F_k^{i+i} - F_k^i}{\Delta s} + G_k^{i+1/2} = 0 \qquad k = 1, 2, 3 \tag{12a}$$

$$G_k^{i+1/2} = \frac{1}{2}\left[G_k^{i+1} + G_k^i\right] \qquad i = 1, N-1 \tag{12b}$$

This gives the following recurrence equation:

$$F_k^{i+1} = F_k^i - \frac{\Delta s}{2}\left[G_k^{i+1} + G_k^i\right] \qquad \begin{matrix} k = 1, 2, 3 \\ i = 1, N-1 \end{matrix} \tag{13}$$

Because G_k is a nonlinear function of forces, moments, curvatures, and angles, an implicit scheme is used where F_k refers to values at iteration $(n+1)$, whereas G_k is calculated using values obtained at the previous iteration (n). A similar form can be easily obtained for the moment equilibrium equation (8) and the compatibility equations (9) and (10).

Then, it is important to note that for the case of cantilevered beams that will be considered here, all forces and moments are known boundary conditions at the tip of the beam, and all angles and displacements are given at the root of the beam

$$F_k^N = 0 \quad \text{and} \quad M_k^N = 0 \qquad k = 1, 2, 3$$

$$\theta^1 = \beta^1 = \psi^1 = 0 \quad \text{and} \quad x^1 = y^1 = z^1 = 0 \tag{14}$$

Under these conditions, the following iterative procedure is then used to integrate these discrete equations:

1) All quantities are initialized to zero.

2) Force and moment equilibrium equations (7) and (8) are integrated from the tip of the beam to the root, i.e., from $i = N - 1$ to $i = 1$, using the relations (13). Note that in the G term in these relations, both curvatures, angles, forces, and moments are present. However, at this step these are kept constant at the value they had at the previous iteration.

3) New curvatures ω_i are calculated using the inverted stress-strain relations (11) and the forces and moments calculated in the preceding step.

4) New angles and displacements are calculated using the preceding compatability equations (9) and (10) discretized in the same way as the equilibrium equations (13), and proceeding now from the root to the tip.

5) A convergence test is applied, and if not met, a new integration iteration is done starting at 2). The following criterion is used:

$$\left|\frac{\Delta x^n}{L}\right|, \quad \left|\frac{\Delta y^N}{L}\right|, \quad \left|\frac{\Delta z^N}{L}\right| < \epsilon$$

with $\epsilon = 10^{-5}$ typically and L = beam length.

Normally, a certain loading is applied to the beam and the corresponding displacements are found directly using this procedure. For certain cases, however, it is necessary to stabilize the iterations by using some form of underrelaxation, especially when axial loads (either tensile or compressive) are present. It is also possible to use an incremental loading by starting step 1) with the solution obtained at the preceding load level. When using underrelaxation, the following modification is done at step 4) when updating the angles. Normally,

$$[\theta^{i+1}]^{n+1} = [\theta^i]^{n+1} + [\Delta\theta^{i+(1/2)}]^n$$

which becomes

$$[\theta^{i+1}]^{n+1} = (1 - \sigma)[\theta^{i+1}]^n + \sigma([\theta^i]^{n+1} + [\Delta\theta^{i+(1/2)}]^n) \tag{15}$$

where σ is the underrelaxation factor, from 1 (no underrelaxation) to 0 (no increment for θ^{i+1}), and n is the iteration number. An identical formula is used for β and ψ.

The choice of a value for σ is given primarily by experience and is mostly affected by the magnitude of the axial load applied to the beam, for instance, through centrifugal forces. in that case, the higher the loads, the lower the σ used. Typical values ranged from 1 to 0.3.

Once new angles have been calculated with underrelaxation, it is necessary to calculate, using Eqs. (5), a new value for the three curvatures based on the new angles in order to still satisfy exactly the compatability relations. If that is not done, the integration of the equilibrium equations (7) and (8) will be incorrect and lead to an unstable scheme in the presence of axial loads.

Applied Loads

As an example, two kinds of loadings are considered here as applied on the blades. The first one is simply gravity and the blade's own weight, which will appear in the term

$$p_3^G = -mg \tag{16}$$

where m is the blade mass per unit length and g the gravity constant.

The next type of loading consists of centrifugal forces or, more precisely, their time-independent component. We assume that the global axes (X, Y, Z) are rotating at a constant angular velocity Ω and use the well known relation to define the force acting on a volume element dV in a rotating coordinate system (Fig. 3)

$$dF = -\rho[\Omega \times (\Omega \times r)]\, dV \tag{17}$$

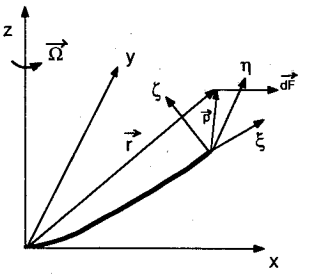

Fig. 3 Centrifugal forces.

where ρ is the mass density and Ω the rotation vector around the Z axis.

$$r = (x, y, z)^T + [T]^T(0, \eta, \zeta)^T \tag{18a}$$

$$r = (x, y, z)^T + (T_{21}\eta + T_{31}\zeta, T_{22}\eta + T_{32}\zeta, T_{23}\eta + T_{33}\zeta)^T \tag{18b}$$

Note that the first part of the preceding position vector represents the position of the center of the cross section and the second part the position in the global axes of a point (ξ, η) on that cross section.

Integrating this force (17) over the cross section gives the force resultant per unit length defined in global axes. But first we list the definition of some well-known quantities

$$\iint_A \rho\eta \, d\eta \, d\zeta = m\eta_{cg}, \qquad \iint_A \rho\zeta \, d\eta \, d\zeta = m\zeta_{cg}$$

$$\iint_A \rho\eta^2 \, d\eta \, d\zeta = I_{\zeta\zeta}, \qquad \iint_A \rho\zeta^2 \, d\eta \, d\zeta = I_{\eta\eta}$$

$$\iint_A \rho\eta\zeta \, d\eta \, d\zeta = I_{\eta\zeta}$$

If we use these quantities, centrifugal forces are expressed as

$$p_1^G = \Omega^2 m[x + T_{21}\eta_{cg} + T_{31}\zeta_{cg}] \tag{19a}$$

$$p_2^G = \Omega^2 m[y + T_{22}\eta_{cg} + T_{32}\zeta_{cg}] \tag{19b}$$

$$p_3^G = 0 \tag{19c}$$

Similarly, centrifugal moments can be calculated by taking the moment around the center of the cross section

$$dm^G = p \times dF \quad \text{with} \quad p = \begin{bmatrix} T_{21}\eta + T_{31}\zeta \\ T_{22}\eta + T_{32}\zeta \\ T_{23}\eta + T_{33}\zeta \end{bmatrix}$$

$$m_1^G = -\Omega^2 \begin{bmatrix} my(T_{23}\eta_{cg} + T_{33}\zeta_{cg}) + T_{22}T_{23}I_{\zeta\zeta} + T_{32}T_{33}I_{\eta\eta} \\ + (T_{32}T_{23} + T_{22}T_{33})I_{\eta\zeta} \end{bmatrix} \tag{20a}$$

$$m_2^G = +\Omega^2 \begin{bmatrix} mx(T_{23}\eta_{cg} + T_{33}\zeta_{cg}) + T_{21}T_{23}I_{\zeta\zeta} + T_{31}T_{33}I_{\eta\eta} \\ + (T_{23}T_{31} + T_{21}T_{33})I_{\eta\zeta} \end{bmatrix} \tag{20b}$$

$$m_3^G = +\Omega^2[\, my(T_{21}\eta_{cg} + T_{31}\zeta_{cg}) - mx(T_{22}\eta_{cg} + T_{32}\zeta_{cg})] \tag{20c}$$

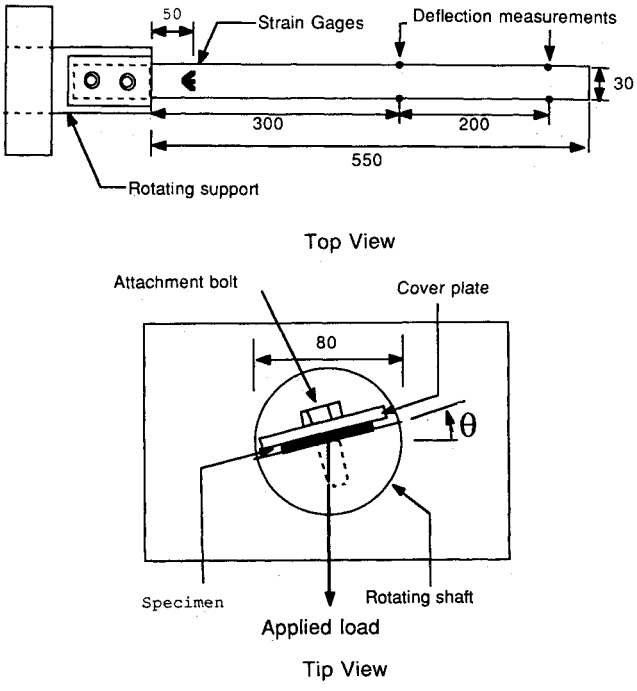

Fig. 4 Static tests' setup (all dimensions in mm).

Table 1 AS4/3501-6 ply properties

$E_1 = 142$ GPa
$E_t = 9.8$ GPa
$G_{1t} = 6$ GPa
$\nu_{1t} = 0.3$
$t_{ply} = 0.134$ mm
$\rho = 1580$ kg/m^3

Table 2 Laminate properties

$[0/90]_{3s}$ laminate	$t = 1.49 \times 10^{-3}$ m	
$E_{11} = 3.7 \times 10^6$ N	$E_{22} = 2.6 \times 10^5$ N	$E_{33} = 2.9 \times 10^5$N
$E_{44} = 0.183$ Nm^2	$E_{55} = 0.707$	Nm^2 $E_{66} = 276$ Nm^2
$[45/0]_{3s}$ laminate	$t = 1.47 \times 10^{-3}$ m	
$E_{11} = 4.0 \times 10^6$ N	$E_{22} = 2.6 \times 10^5$ N	$E_{33} = 5.5 \times 10^5$ N
$E_{44} = 0.368$ Nm^2	$E_{55} = 0.522$ Nm^2	$E_{66} = 298$ Nm^2
$E_{12} = 2.7 \times 10^5$ N	$E_{45} = 0.102$ Nm^2	
$[20/-70/-70/20]_{2a}$ laminate	$t = 1.92 \times 10^{-3}$ m	
$E_{11} = 3.9 \times 10^6$ N	$E_{22} = 1.1 \times 10^6$ N	$E_{33} = 1.2 \times 10^5$ N
$E_{44} = 1.18$ Nm^2	$E_{55} = 0.983$ Nm^2	$E_{66} = 290$ Nm^2
$E_{14} = 522$ Nm		

Note: in more conventional terms, $E_{11} \approx EA$, $E_{22} \approx GA_\eta$, $E_{33} \approx GA_\zeta$, $E_{44} \approx GJ$, $E_{55} \approx EI_\eta$, $E_{66} \approx EI_\zeta$, $E_{12} \approx$ extension-shear coupling, $E_{14} \approx$ extension-twist coupling, $E_{45} \approx$ bending-twist coupling.

Experiments

Several experiments were performed to verify the analytical models presented in the preceding section. These experiments consisted of a series of static bending tests on several cantilevered flat beams of various layups.

During the static tests, the specimens were mounted in the fixture, shown in Fig. 4, which consisted of several elements. First, a stiff aluminum base was attached to a "strong back" by two bolts. This base contains holes into which an aluminum shaft is fitted. This shaft can be rotated so that the root of the beam is positioned at a variable angle in the vertical direction and is held in place with a screw. The outer end of the shaft is flattened over a 50 mm portion where the specimen is placed. An aluminum top plate is then placed over the root of the specimen and tightened with two bolts. The beam is aligned and made horizontal with a level. The strain gauges are connected to a gauge box. Under the beam, a sheet of graph paper is placed on a table that is also made horizontal with a level. A variable load consisting of different weights is applied at the tip of the beam. For each load, the value of all six gauges is recorded; by using a square angle placed on the table, the vertical deflection of four points on the beam (two on each side, as indicated in Fig. 4) is also recorded, as well as the vertical projection of these points on the graph paper sheet, in order to measure the displacements of these points in all three directions. For each beam, the tests are first performed with the root of the beam horizontal and then with the root of the beam turned at an angle of 45 and -45 deg.

Constitutive Properties

Before describing the analytical and experimental results, it is necessary to define some of the material properties used for the examples next presented. The basic (nominal) ply properties of the AS4-3501/6 graphite/epoxy are given in Table 1. Classical laminated plate theory is then used to calculate the laminate properties of each layup used, and the results for the layups used here are shown in Table 2. It is important to note that the basic ply properties used were obtained from static tensile tests only. For the bending and dynamic behavior of thin laminates, it is often suggested that these properties should be modified and, in general, reduced. In this investigation, however, it was found that this modification was apparently not necessary: When examining such a thin laminate after cure, it was noted that a layer of epoxy (from the bleeding process) covers both sides of the whole laminate. By using a fine grit sand paper to remove most of that layer and measuring the laminate thickness before and after doing so, it was found that these two layers (i.e., on both faces) are about 0.1 to 0.2 mm thick. Therefore, the load-carrying section of the laminate is actually smaller than what is measured normally. This might not sound like a large difference, but compared, for example, to laminate nominally 1.6 mm thick, a 0.2 mm reduction represents a 12% change, but more importantly, it represents a 32% reduction in bending stiffness (which is a function of the cube of the laminate thickness). Therefore, the thickness reported for all the laminates and used in calculating the specimens' constitutive properties shown in Table 2 is the value measured after removal of the epoxy layers.

Analytical and Experimental Results

The results from the static model are described in this section. By using the preceding material properties and the actual specimen dimensions as input, the static analysis program is run with a variable-applied tip load. All of the runs were made on DEC MicroVax II computer and each analysis with about 10 load levels takes approximately 30 to 60 s of CPU time, longer times being required for cases with larger deflections. The beam length was divided into 56 discrete nodes for plotting convenience, but as little as 15 nodes are usually sufficient to obtain an accurate solution. An underrelaxation factor of 0.9 was used and each load case took between 5 and 18 iterations to converge.

Several types of flat beam specimens, 560 mm by 30 mm, were used in the static test to illustrate the effects of some of the structural coupling terms. Flat beam specimens were chosen because of their low bending stiffness, which allows them to reach very large displacements without any structural failure. The first specimen has a $[0/90]_{3s}$ layup, without any coupling to serve as a reference. The next one is a $[45/0]_{3s}$, to illustrate the effect of bending-twisting coupling, whereas a $[20/-70/-70/20]_{2a}$ layup was used to illustrate the effect of extension-twist. This last layup also has the interesting property of not having any thermal residual curvature while being an antisymmetric layup.

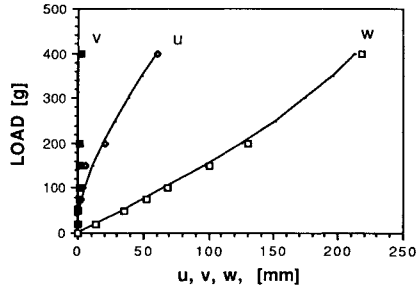

Fig. 5 Comparison between analysis (lines) and experimental data (symbols) for a $[0/90]_{3s}$ beam with its root at 0 deg.

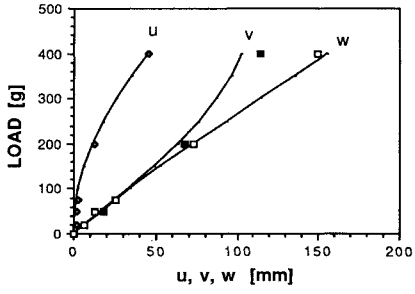

Fig. 6 Comparison between analysis (lines) and experimental data (symbols) for a $[0/90]_{3s}$ beam with its root at 45 deg.

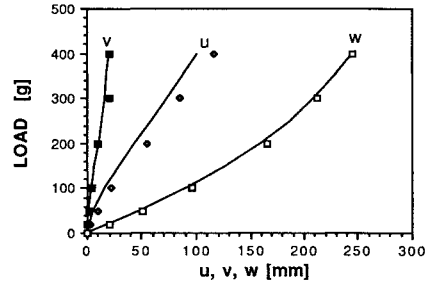

Fig. 7 Comparison between analysis (lines) and experimental data (symbols) for a $[45/0]_{3s}$ beam with its root at 0 deg.

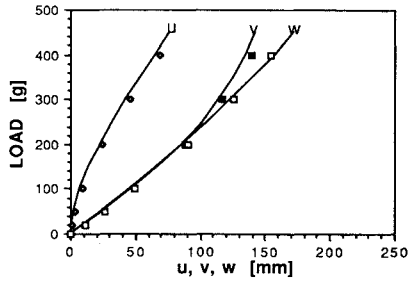

Fig. 8 Comparison between analysis (lines) and experimental data (symbols) for a $[45/0]_{3s}$ beam with its root at 45 deg.

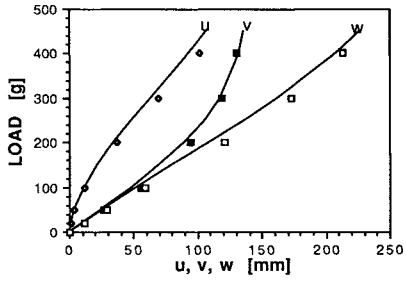

Fig. 9 Comparison between analysis (lines) and experimental data (symbols) for a $[45/0]_{3s}$ beam with its root at -45 deg.

In Fig. 5, the measured displacements u and w for the $[0/90]_{3s}$ specimen, with its root oriented at 0 deg are plotted vs the tip load. Note that these displacements are measured at a station located 500 mm from the root, and that u is actually negative and v is zero in this case. The initial behavior for w is fairly linear and tends to stiffening as the load increases up to a maximum tip deflection of about 40% of the beam length. As expected from the linear solution, u is initially very small and the tip of the beam starts moving in toward the root only when significant rotations are obtained. The error rate for the u displacement is slightly higher than for the other displacements because the analysis results for u are more sensitive to the beam initial shape (i.e., before loading). For instance, running the analysis with a beam initially straight or slightly curved makes some difference for u but not much for v or w. In the results presented here, the beam's own weight is included but not the beam residual curvature from manufacturing, and all displacements are measured from that initial position (as in the experiments). In Fig. 6, the root of the beam has been turned to an angle of 45 deg. In this case, all three displacements are present and u is again negative (as in all of the following figures). Here, since the bending stiffness around the strong axis is so much greater than around the weak axis, most of the displacement occurs in a 45 deg direction, that is, by bending around the weak axis, so that the v and w displacements are initially equal. However, as the load and displacements increase, a twisting moment develops in the beam that tends to turn the beam weak axis toward a more horizontal position, thereby increasing the vertical displacement w. As one can see, the agreement between the experimental data and analysis is excellent, even at the highest loads where the nonlinearities become more significant.

The next set of examples illustrates some of the data taken for the $[45/0]_{3s}$ beam. The measured tip displacements u, v, w for that beam with its root at a 0 deg angle are shown in Fig. 7. The most striking difference when comparing this plot with the similar one shown for the $[0/90]_{3s}$ beam is the presence of a significant v displacement. This is a good illustration of a consequence of the bending-twisting coupling present in this beam: As the tip load is increased, bending moments are created in the beam that cause it to twist. Then, since the cross section is rotated, displacements occur in the horizontal as well as the vertical plane since the beam tends to bend around its weak axis. Also, as in the preceding case, the large displacements tend to reduce w and increase u. In Fig. 8, the root of the beam is rotated to an angle of $+45$ deg, and then in Fig. 9 to a -45 deg angle. Note that v is positive in Fig. 8 and negative in Fig. 9. Although the behavior with the root at a $+45$ deg or -45 deg was virtually identical for the $[0/90]_{3s}$ beam, a comparison of the two figures reveals quite different behavior for this beam. In the $+45$ deg case, v and w remain equal for most of the loading, whereas for the -45 deg case, they become different very rapidly. This is again a consequence of the bending-twist coupling. In the $+45$ deg case, the twist caused by the tip load and the large deflections is com-

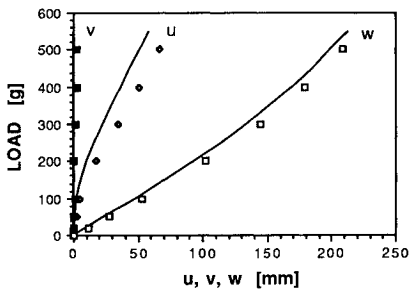

Fig. 10 Comparison between analysis (lines) and experimental data (symbols) for a $[20/-70_2/20]_{2a}$ beam with its root at 0 deg.

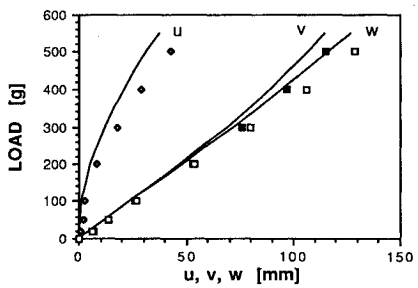

Fig. 11 Comparison between analysis and experiments for a $[20/-70/-70/20]_{2a}$ beam with its root oriented at 45 deg.

pensated by the twist from the coupling effect so that the cross section does not rotate very much and bending occurs mostly in the +45 deg direction. In the −45 deg case, however, the twists from both effects add up, causing the cross section to rotate at an angle less than the initial 45 deg angle, thereby causing much larger w displacements. Once again, the agreement between the analysis and the data is very good, with a little offset noticed in certain cases for u or v. The model is able to fully take into account the strong bending-twist coupling present in this layup.

The last example shown here is the $[20/-70/-70/20]_{2a}$ beam. The results with the root at a 0 deg angle are shown in Fig. 10. The results are qualitatively very similar to those of the $[0/90]_{3s}$ specimen, and the extension-twist coupling does not have very much influence here since the axial load is very small. The results for the case with the root at a +45 deg angle are shown in Fig. 11; the results for the −45 deg case are virtually identical and are not shown here. When compared with the results of the $[0/90]_{3s}$ specimen, one can see that v and w tend to remain equal longer (i.e., up to larger deflections); this is due, in part, to the fact that this layup has a much higher torsional stiffness than the $[0/90]_{3s}$ layup and therefore tends to twist less under the tip load.

Conclusion

An analytical model capable of analyzing the large deflection behavior of beams with structural couplings is presented. Euler angles are used to describe the beam deformed position and to derive equilibrium and compatability equations without any ordering scheme. The iterative solution procedure used to solve these equations is fast and accurate. A series of bending tests performed on several graphite/epoxy cantilevered thin beams illustrate well the large deflection behavior of flexible blades. The data obtained compare very well with the analytical results and will provide useful reference cases.

Acknowledgments

This research was supported by U.S. Army Research Office Contract DAAL03-87-K-0024, with Gary Anderson as Technical Monitor.

References

[1]Nixon, M. W., "Improvement to Tilt Rotor Performance Through Passive Blade Twist Control," NASA TM 100583, April 1988.

[2]Lake, R. C., and Nixon, M. W., "A Preliminary Investigation of Finite Element Modeling for Composite Rotor Blades," NASA TM 100559, Jan. 1988.

[3]Hodges, R. V., and Nixon, M. W., "Comparison of Composite Rotor Blade Models: a Coupled-Beam and an MSC-NASTRAN Finite-Element Model," NASA TM 89024, March 1987.

[4]Houbolt, J. C., and Brooks, G. W., "Differential Equations of Motion for Combined Flapwise Bending, Chordwise Bending, and Torsion of Twisted Non-Uniform Rotor Blades," NACA Rept. 1346, 1958.

[5]Isakson, G., and Eisely, J. G., "Natural Frequencies in Coupled Bending and Torsion of Twisted Rotating and Nonrotating Blades," NASA CR-65, July 1964.

[6]Friedmann, P. P., "Recent Developments in Rotary-Wing Aeroelasticity," *Journal of Aircraft,* Vol. 14, No. 11, 1977, pp. 1027–1041.

[7]Friedmann, P. P., "Recent Trends in Rotary-Wing Aeroelasticity," *Vertica,* Vol. 11, Jan. 1987.

[8]Hodges, D. H., and Dowell, E. H., "Nonlinear Equations of Motion for the Elastic Bending and Torsion of Twisted Non-Uniform Rotor Blades," NASA TN D-7818, Dec. 1974.

[9]Hong, C. H., and Chopra, I., "Aeroelastic Stability of a Composite Rotor Blade," *Journal of the American Helicopter Society,* Vol. 30, April 1985.

[10]Rosen, A., and Friedmann, P. P., "The Non-Linear Behavior of Elastic Slender Straight Beams Undergoing Small Strains and Moderate Rotations," *Journal of Applied Mechanics,* Vol. 46, March 1979.

[11]Bauchau, O. A., and Hong, C.-H., "Finite Element Appoach to Rotor Blade Modelling," *Journal of the American Helicopter Society,* Vol. 32, Jan. 1987.

[12]Hinnant, H. E., and Hodges, D. H., "Nonlinear Analysis of a Cantilever Beam," *AIAA Journal,* Vol. 26, No. 12, 1988.

[13]Minguet, P. J., "Static and Dynamic Behavior of Composite Helicopter Rotor Blades Under Large Deflections," Ph.D. Thesis, Dept. of Aeronautics and Astronautics, MIT, Cambridge, MA, May 1989; also TELAC Rept. 89-7, MIT, May 1989.

[14]Rivello, R. M., *Theory and Analysis of Flight Structures,* McGraw-Hill, New York, 1969.